

A phenomenological model for thermally-induced hysteresis in polycrystalline shape memory alloys with internal loops

Journal of Intelligent Material Systems
and Structures
1–12

© The Author(s) 2021

Article reuse guidelines:

sagepub.com/journals-permissions

DOI: 10.1177/1045389X211048228

journals.sagepub.com/home/jim



Yuxiang Han¹ , Haoyuan Du¹, Linxiang Wang¹ and Roderick Melnik²

Abstract

In the current study, a 1-D phenomenological model is constructed to capture the temperature-induced hysteretic response in polycrystalline shape memory alloys (SMAs). The martensitic and austenitic transformations are regarded as the first-order transitions. A differential single-crystal model is formulated on the basis of Landau theory. It is assumed that the transformation temperatures follow the normal distribution among the grains due to the anisotropic stress field developed in the material. The polycrystalline hysteretic response is expressed as the integration of single-crystal responses. Besides, the prediction strategy for incomplete transitions is presented, and the first-order reversal curves are obtained via density reassignment. The proposed model is numerically implemented for validation. Comparisons between the modeling results and the experimental ones demonstrate the capability of the proposed model in addressing the hysteresis in thermally-induced phase transformations.

Keywords

Shape memory alloy, Landau theory, phase transformation, thermally-induced hysteresis, internal loops

1. Introduction

Shape memory alloys (SMAs) refer to a class of metallic alloys, which possess the ability to revert to their original shape upon heating. The underlying mechanism for this shape memory behavior is the diffusionless, first-order transformation between austenite and martensite, which can be induced by either temperature or stress. As a consequence of cyclic thermomechanical loading, that is, training, SMAs exhibit the two-way shape memory effect (TWSME). TWSME refers to the thermally-induced phase transition accompanied by the reversible strain output without the requirement of any external mechanical load. A variety of models have been proposed to study the thermally-induced hysteresis and the transformation-induced plasticity (TRIP) in training for decades.

Phenomenological models for phase transitions rely on macroscopic analysis with simplified homogenization techniques where the model parameters are commonly determined by direct experimental observations or macro-scale data fitting. One approach is to address the material response at the local grain-level and extend the grain-level response to the poly-crystal level via some statistical distribution properties, such as the

homogenized energy model (Crews et al., 2012; Massad and Smith, 2005). The other approach is to derive the constitutive relation through continuum thermodynamics. It should be noted that most studies on the thermally-induced phase transition are to model the TRIP in training with thermodynamics and predict the thermal hysteretic responses under cyclic loading (Heller et al., 2019; Oliveira et al., 2018; Saleeb and Owusu-Danquah, 2017). More recent phenomenological studies focus on the cyclic behavior (Petrini and Bertini, 2020; Xiao and Jiang, 2020), the functional fatigue (Bartel et al., 2017; Chemisky et al., 2018; Dornelas et al., 2020), and the design of SMA actuators (Hao et al., 2017; Scalet et al., 2019). Besides, the material displays the pattern of minor loops or internal

¹State Key Laboratory of Fluid Power and Mechatronic Systems, Zhejiang University, Hangzhou, China

²MS2Discovery Interdisciplinary Research Institute, Wilfrid Laurier University, Waterloo, ON, Canada

Corresponding author:

Linxiang Wang, State Key Laboratory of Fluid Power and Mechatronic Systems, Zhejiang University, No. 38, Road Zheda, Hangzhou 310027, China.

Email: wanglx236@zju.edu.cn

loops when it undergoes incomplete phase transitions. Most phenomenological schemes for internal-loop prediction depend on the evolution of the phase fractions that are incorporated into the constitutive relation to estimate the extent of transition (Bo and Lagoudas, 1999; Chemisky et al., 2011; Doraiswamy et al., 2011; Rao et al., 2014). It should be noted that most of the phenomenological models delineate the phase transition by the evolution of internal variables and those thermodynamic models often require the numerical implementation to determine the evolution kinetics. Moreover, most of them are not formulated in differential equations, which makes them inconvenient for the control of SMAs.

In recent decades, as an emerging phenomenological technique (Mamivand et al., 2013), phase-field models numerically simulate the evolution of microstructures and predict the macroscopic response in SMAs. Most early studies resorted to Landau theory of phase transformation to theoretically investigate the responses of SMAs (Falk, 1980, 1983). Phase-field models use a set of field variables and determine the evolution of the field variables via the Time-Dependent Ginzburg-Landau (TDGL) equation (Cissé and Asle Zaeem, 2020b; Daghia et al., 2010; Dhote et al., 2015; She et al., 2013; Zhong and Zhu, 2014). In particular, phase-field modeling has been recently deployed to investigate more challenging tasks, such as transformation-induced plasticity (TRIP) (Cissé and Asle Zaeem, 2020a; Xie et al., 2019) and tension-compression asymmetry (Li and Su, 2020), etc. Generally, phase-field modeling provides a flexible framework to study the dynamic microstructure evolution with a set of partial differential equations (PDEs), which often require intensive computation. The sophisticated formulation makes it unsuitable for the control of SMA actuators.

Most phenomenological models are aimed to capture the macroscopic response via thermodynamics while phase-field models are conducted for the simulation of microstructural evolution. However, both of them are incompetent for the control of SMAs due to their inappropriate model formulation. To facilitate the control of SMAs and improve the computational efficiency, a 1-D differential model is proposed to capture the hysteretic phenomenon in the thermally-induced transformation for the SMA polycrystal. Besides, motivated by the scaling policy for internal loops (Rizzello et al., 2019) that utilizes the geometrical similarity between the outer loop and the inner ones, a strategy is proposed to involve both geometrical and physical considerations for the prediction of incomplete transitions. The major contribution of this work is remarked as follows. Firstly, a 1-D phenomenological model is constructed focusing on the thermally-induced hysteretic behavior of the material, where the well-known TDGL equation governs the dynamics of phase transition.

Since this work emphasizes the macroscopic hysteretic response rather than the microstructural evolution, non-local energy terms are neglected and the TDGL equation is expressed in an ordinary differential equation (ODE), which largely reduces the computational cost. Moreover, unlike the classical phase-field framework, the material inhomogeneity is incorporated in a phenomenological way, which is to take into account the variation of model parameters. In this article, the transformation temperatures among grains are employed to quantify the inherent polycrystalline nature of SMAs. The main upside of the presented model is that it maintains simplicity as well as good accuracy in predicting the thermally-induced hysteresis. Besides, the ODE form and low computational cost make it possible to be implemented in control applications. Secondly, the other contribution is to present a straightforward prediction scheme for incomplete transformations, which is based on the self-similar feature of the reversal curves. The concept of density reassignment is introduced to directly estimate the reversal curves from the major hysteresis loop without simulating the evolution of internal variables. Thus, the computational efficiency is improved. Compared with the geometrical scaling policy, the density reassignment relies on the assumption of distributed transformation temperatures, which enriches the physical aspects of the prediction. The remainder of this paper is organized as follows. In Section 2, the single-crystal model is firstly developed and the differential governing equation is given. In Section 3, the polycrystalline model is constructed by the integration of single-crystal units, which is analyzed on the basis of distributed transformation temperatures. The model calibration procedure is stated in detail and the prediction strategy for incomplete transitions is given in Section 4. Comparisons between the experimental results and the model ones are given in Section 5. In Section 6, this work is concluded and remarked.

2. Single-crystal model

The phase transformation in SMAs induced by thermo-mechanical loadings always exhibits a remarkable hysteresis behavior in the strain response. In this section, a macroscopic model is proposed to describe the hysteresis behavior at the single-crystal level. The model formulation is aimed to capture the uniaxial strain response of the single-crystal SMA specimen under uniaxial stress. Since the heat transfer and the wave propagation patterns are not the primary concern, the material temperature and the uniaxial strain are assumed to be uniform throughout the specimen and the discussion can be further regarded as a 1-D isothermal problem. It should be pointed out that the proposed 1-D model is developed to tackle the

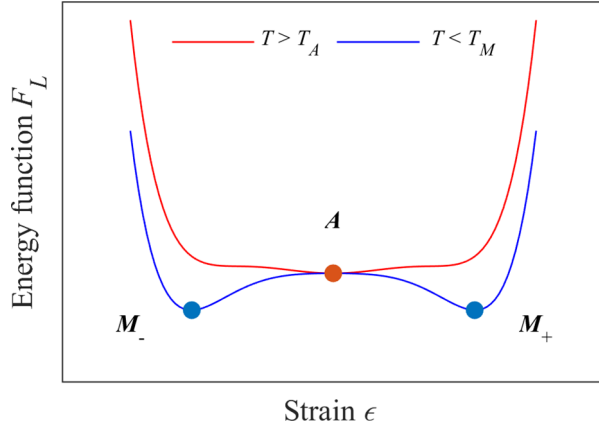


Figure 1. The strain versus the thermodynamic potential F_L at different temperatures.

macroscopic hysteresis in the transition from cubic austenite to tetragonal martensite. However, the proposed model is also valid in the transition from cubic austenite to monoclinic martensite if the material is subjected to uniaxial stress and the macro-scale uniaxial strain response is studied.

The martensitic transformation follows the characteristics of the first-order phase transformation, and the thermodynamic potential is constructed as the Landau free energy function F_L , with respect to the macroscopic strain ε and the material temperature T ,

$$F_L(\varepsilon, T) = \frac{a_2}{2}(T - T_M)\varepsilon^2 - \frac{a_4}{4}\varepsilon^4 + \frac{a_6}{6}\varepsilon^6. \quad (1)$$

Herein, a_2 , a_4 , a_6 are all positive constants to be identified from the experimental data and $a_2(T - T_M)\varepsilon^2$ is the only term that varies linearly with the material temperature. At the single-crystal level, T_M is the stress-free martensitic transition temperature. The stress-free austenitic transition temperature T_A can be expressed as

$$T_A = T_M + \frac{a_4^2}{4a_2a_6}. \quad (2)$$

As shown in Figure 1, the shape of the thermodynamic potential varies with the material temperature and the local extremum represents the austenite phase or the martensite phase. At high temperatures ($T > T_A$), the thermodynamic potential has only one local minimum, which indicates that the austenite (A) is the stable phase. At low temperatures ($T < T_M$), the thermodynamic potential has two local minima, which indicates that the martensite (M) is the stable phase with two energetically-equivalent variants (M_+ and M_-). To introduce the stress dependence of the phase transition, the total free energy function ψ comprises the thermodynamic potential F_L , and the work due to the applied external stress σ , having the following form (Crews et al., 2012; Massad and Smith, 2005):

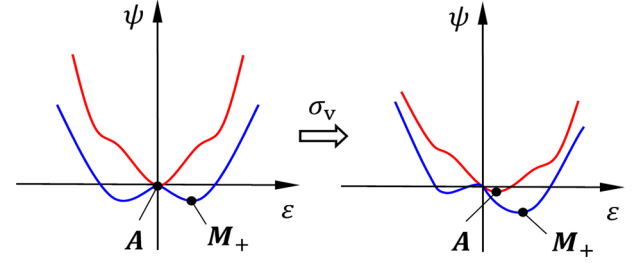


Figure 2. The effect of the stress σ_v on reshaping of the total free energy function.

$$\psi(\varepsilon, \sigma, T) = F_L - \sigma\varepsilon = \frac{a_2}{2}(T - T_M)\varepsilon^2 - \frac{a_4}{4}\varepsilon^4 + \frac{a_6}{6}\varepsilon^6 - \sigma\varepsilon. \quad (3)$$

Since the microstructural evolution is ignored in the proposed macroscopic model, other non-local energy terms, such as the gradient free energy, are not taken into account. It is worth noting that the shape of the total free energy function is influenced by the material temperature and the applied external stress. The equilibria of the free energy function indicate the energetically favored phases. Therefore, the phase transformation is viewed as the switching between the equilibria.

In this paper, the phase transformation at the single-crystal level is governed by the well-known TDGL equation (Mamivand et al., 2013),

$$\frac{d\varepsilon}{dt} = -L \frac{\delta\psi}{\delta\varepsilon}, \quad (4)$$

where the strain ε is selected as the order parameter and the coefficient L is the kinetic constant. The equation above contains the strain-rate term which is proportional to the variational derivative of the total free energy function ψ with respect to the strain ε . It should be clarified that the strain-rate term is introduced as the dissipative effect in the phase transformation to diminish the total free energy function. Therefore, equation (4) governs the hysteretic phase transition with the strain-rate-dependent dissipation, where the evolution of the strain is related to the variation of the total free energy function. Substituting equation (2) into equation (4) gives the following ODE:

$$\tau\dot{\varepsilon} + a_2(T - T_M)\varepsilon - a_4\varepsilon^3 + a_6\varepsilon^5 - \sigma = 0, \quad (5)$$

where $\tau = 1/L$ denotes the coefficient related to the dissipative effect. It is worth noting that the external stress term disappears in the differential governing equation, that is, equation (5), as $\sigma = 0$ under the stress-free thermal loading. In this work, a small but sufficient stress $\sigma = \sigma_v$ is employed to induce the favoritism mathematically in the modeling of the thermally-induced hysteresis under the stress-free condition. It can be seen in Figure 2 that two martensitic variants are energetically

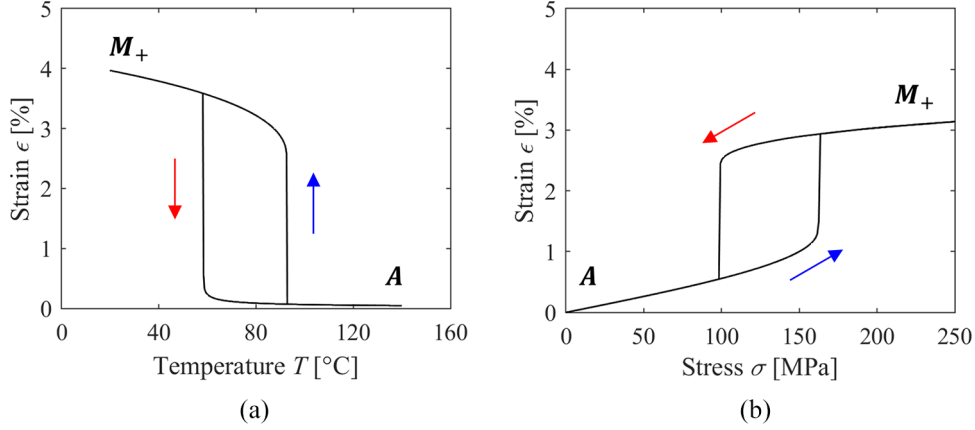


Figure 3. Simulation of the hysteretic response via the single-crystal model: (a) the strain-temperature hysteresis and (b) the strain-stress hysteresis.

identical under the zero-stress condition due to the symmetry of the Landau free energy function. The stress term σ_v serves as the perturbation which reshapes the free energy function and leaves one martensitic variant stable and the other one metastable. Hence, the stable variant is energetically favored and the corresponding transition is initiated through the introduction of σ_v . Since the magnitude of σ_v is small enough, the corresponding influence could be ignored and the simulation results could be approximately viewed as the temperature-induced strain under zero-stress condition. In this article, σ_v is chosen as a random value between 0 and 0.01 MPa. An example of a stress-free thermally-induced A to M_+ transition is given in Figure 3(a) with the parameter set: $a_2 = 4.2 \times 10^2$, $a_4 = 4.7 \times 10^7$, $a_6 = 3.6 \times 10^{10}$, $T_M = 56$, and $\tau = 0.83$, where the hysteresis loop is roughly captured by the proposed model. It should be clarified that the governing equation is established based on the energy principle, and therefore, it is not limited to thermally-induced transition. Isothermal stress-induced transition can be described via the presented model as well. A stress-strain hysteresis loop for the uniaxial tensile test is shown in Figure 3(b) using the above parameter set, which also portrays the transition from A to M_+ .

It is worth noting that the proposed single-crystal model is stress-dependent for strain-temperature hysteresis due to the incorporation of the stress-related term. Examples of the strain-temperature hysteresis under different bias stresses are simulated with the parameter set: $a_2 = 3.17 \times 10^4$, $a_4 = 4.26 \times 10^9$, $a_6 = 2.38 \times 10^{12}$, $T_M = 35.7$, and $\tau = 0.062$, as shown in Figure 4. The stress-dependent property can be well described from the perspective of the energy principle. The strain-rate term in equation (4) vanishes yielding $\delta\psi/\delta\dot{\epsilon} = 0$, which gives the condition for the equilibrium states. As is mentioned, the phase transition is associated with the switching between the equilibria. The stability of the equilibrium changes as the switching occurs. For

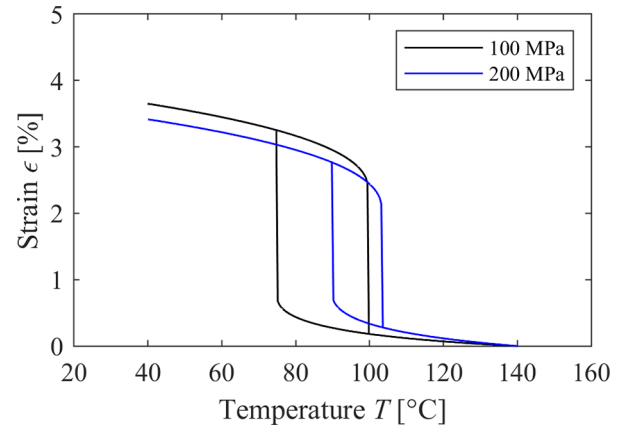


Figure 4. Simulation of the strain-temperature hysteresis under different bias stresses.

thermally-induced transitions, the austenite phase loses its stability during cooling and the martensite phase becomes unstable upon heating. The phase transition is then explained as the change in the stability of the equilibrium and the condition $\delta^2\psi/\delta\epsilon^2 = 0$ need to be satisfied. Thus, the phase transition occurs when both $\delta\psi/\delta\epsilon = 0$ and $\delta^2\psi/\delta\epsilon^2 = 0$ are satisfied. The external stress makes a difference in the total free energy function, resulting in that the hysteresis response varies with the applied stress.

3. Polycrystalline model

Hysteresis nonlinearities in the thermally-induced cases are roughly captured by the differential single-crystal model, as is plotted in Figure 3(a). Nonetheless, it is noticeable that the single-crystal model exhibits a sudden increase or decrease in the strain value during the phase transformation while the actual experimental result displays a smooth and gradual transition in strain. In order to compensate for this drawback, the

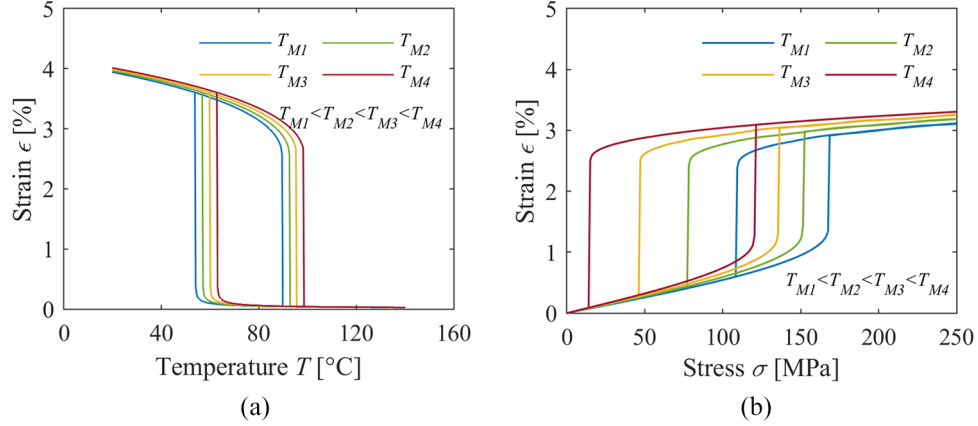


Figure 5. Simulation of the hysteretic responses with different T_M 's: (a) the thermally-induced hysteresis and (b) the stress-induced hysteresis.

single-crystal model is extended to the polycrystalline case in this section, where the polycrystalline hysteresis is constructed as the weighted sum of the single-crystal responses.

TWSME refers to the capability of SMA to switch between austenite and oriented martensite upon heating or cooling without requiring any mechanical load, which is realized by repeated thermomechanical loadings, that is, training. For the trained SMA polycrystals, an anisotropic stress field is developed among the material. It is well acknowledged that the phase transformation temperatures are macroscopically stress-influenced, which is based on experimental observation (Maletta et al., 2008). Hence, it is assumed in this article that the phase transformation temperatures vary from grain to grain as a consequence of this stress field. It is worth noting that the assumption is also valid in modeling the stress-assisted thermal hysteresis of the untrained SMA polycrystals. As is mentioned in Section 2, T_M is the critical point at which the grain-level martensitic transformation starts in the absence of external stress. The variation of T_M can effectively affect the free energy function, yielding different hysteretic strain responses among grains, as is shown in Figure 5(a). Therefore, the varying material parameter T_M is employed here to represent the material inhomogeneity. Even though this paper mainly discusses the thermally-induced hysteresis in polycrystalline SMAs, it should be noted that the presented strategy can be also extended to the simulation of the isothermal stress-induced hysteresis. When the material is loaded at a high temperature, the hysteretic behavior between stress and strain is observed. The hysteresis loops change with the material parameter T_M , as plotted in Figure 5(b).

In order to incorporate the intrinsic material inhomogeneity in the SMA polycrystals, the polycrystalline response is regarded as the weighted combination of all

the grain-level responses. The grain-level responses are determined with different transformation temperatures and the transformation temperatures are presumed to follow a particular distribution pattern. Besides, the formation of martensitic variants also affects the thermally-induced macroscopic shape change. The variants M_+ and M_- are considered in the proposed 1-D model. M_+ refers to the stable variant under tension while M_- refers to the stable variant under compression. The grain-level strain responses ε_{m+} and ε_{m-} (the subscript “m” indicates that the strain derived with a certain value of T_M and the subscripts “+” and “-” denote the variants M_+ and M_- respectively) for the variants are obtained by the single-crystal model as

$$\tau \dot{\varepsilon}_{m+} + a_2(T - T_M)\varepsilon_{m+} - a_4\varepsilon_{m+}^3 + a_6\varepsilon_{m+}^5 - \sigma_+ = 0, \quad (6-a)$$

$$\tau \dot{\varepsilon}_{m-} + a_2(T - T_M)\varepsilon_{m-} - a_4\varepsilon_{m-}^3 + a_6\varepsilon_{m-}^5 - \sigma_- = 0, \quad (6-b)$$

where σ_+ and σ_- denote the uniaxial tensile stress and compressive stress of the same magnitude, that is, $\sigma_- = -\sigma_+$. It is evident that $\varepsilon_{m-} = -\varepsilon_{m+}$ due to the intrinsic symmetry of the governing equation. Thus, the total strain ε_+ , ε_- of the corresponding variants are then evaluated as the integration of all the grain-level responses as

$$\varepsilon_+ = \int_{\Omega} \varepsilon_{m+} \lambda(T_M) dT_M, \quad (7-a)$$

$$\varepsilon_- = \int_{\Omega} \varepsilon_{m-} \lambda(T_M) dT_M = -\varepsilon_+, \quad (7-b)$$

where Ω is the range of the martensitic transformation temperature T_M and $\lambda(\cdot)$ denotes the corresponding probability density function. In this work, it is

presumed as the normal density function (Bhattacharyya and Lagoudas, 1997)

$$\lambda(x) = \frac{1}{\sqrt{2\pi}\eta} \exp\left(-\frac{(x-\mu)^2}{2\eta^2}\right), \quad (8)$$

where μ and η are coefficients to be estimated from experimental calibration. For the materials that do not follow the assumption of normal distribution, one can modify the probability density function based on experimental observation. The polycrystalline response is then expressed as the weighted combination of the responses of two variants,

$$\varepsilon = \beta \varepsilon_+ + (1 - \beta) \varepsilon_-, \quad (9)$$

where $\beta \in [0, 1]$ is the volume fraction of M_+ after the phase transformation completes. Substituting equation (7) into equation (9) gives the polycrystalline model

$$\varepsilon = \int_{\Omega} (2\beta - 1) \varepsilon_m + \lambda(T_M) dT_M. \quad (10)$$

It is worth noting that β is the stress-dependent factor that affects the ultimate strain output in the polycrystal. The coefficient β is employed to quantify the material configuration after the complete transition and bring the stress-dependence into the proposed model. As is mentioned, M_+ is the stable variant under tension. The increasing tensile load benefits the formation of M_+ and leads to an increase in the value of β . Herein, β is assumed to vary linearly between 0 and 1 with the applied stress as

$$\beta = \begin{cases} 0, & \sigma \leq -\beta_0/k_\sigma \\ \beta_0 + k_\sigma \sigma, & -\beta_0/k_\sigma < \sigma < (1 - \beta_0)/k_\sigma \\ 1, & \sigma \geq (1 - \beta_0)/k_\sigma \end{cases}, \quad (11)$$

where $\beta_0 \in [0, 1]$ is the volume fraction of M_+ after the complete stress-free transition and k_σ is the positive stress influence constant. The presumed stress dependence ensures the volume fraction of M_+ increases as the external tensile stress is elevated. It should be noted that the linear stress dependence is adopted for simplicity. One can use nonlinear functions to quantify the stress dependence of β as well. Thus, the stress-dependent property results from the proposed model in a combined manner. On one hand, the stress dependence is incorporated in the single-crystal model as the contribution to the total free energy function, which leads to the stress-dependent hysteretic response. On the other hand, the factor β that varies with the applied stress is also introduced to influence the polycrystalline strain response.

4. Numerical validation

4.1. Model calibration

In previous sections, the differential single-crystal model and the extended polycrystalline model are developed and discussed schematically. In this section, the procedure of numerical implementation is presented to explain the calibration of the model parameters. The polycrystalline hysteresis is captured by the combination of different single-crystal responses in the current paper. Each of the single-crystal hysteresis units that comprise the polycrystalline response is numerically solved with a set of a_2, a_4, a_6, τ , and a pre-specified T_M . In practice, the estimated values of a_2, a_4 , and a_6 are always so large that equation (5) is a stiff ODE. The MATLAB built-in function *ode23t* solves the stiff problems accurately and efficiently via the trapezoidal method, so that *ode23t* is utilized here to obtain the numerical solution of equation (5). Besides, the parameters β_0 and k_σ plays a significant role in the construction of the polycrystalline hysteresis as well. Therefore, only six model parameters ($a_2, a_4, a_6, \tau, \beta_0$, and k_σ) need to be identified for model calibration. Herein, the model parameters are identified to achieve the least-square error between the experimental data and the model prediction as

$$\min_{\text{mod. para.}} G = \sum_{k=1}^M (\bar{\varepsilon}_k - \varepsilon_k)^2, \quad (12)$$

where $\bar{\varepsilon}_k$'s and ε_k 's are the sampled strain values in the experiment and the relevant simulated values by model prediction and M is the number of the sample points.

Since the proposed model exhibits great nonlinearity, it is essential to find a reasonable set of initial values to achieve good agreement between the experimental data and the model prediction. The parameter identification is carried out in the following procedure to improve the model accuracy, where the prediction error is optimized by the built-in MATLAB function *fminsearch*. Firstly, the single-crystal model is employed to identify the model parameters. The simulated single-crystal response is compared with the experimental data to determine the initial estimation of the model parameters. This set of parameters will be used as the initial value for the next step to facilitate the parameter identification. Secondly, the model parameters are updated with the polycrystalline model. The prediction error is re-optimized to improve the model accuracy. It is worth noting that the integral in the polycrystalline model, that is, equation (10), is computed using the piecewise four-point Gaussian quadrature. The domain of integration in equation (10) is divided into some sub-intervals and the integral over the i -th sub-interval is calculated by four-point Gaussian quadrature. Thus,

the integral over the entire domain is derived as the sum of the integrals over these sub-intervals and the discretized polycrystalline model is given as

$$\varepsilon = (2\beta - 1) \sum_{i=1}^N \sum_{j=1}^4 (\varepsilon_m +)_j^i \lambda_j^i w_j^i. \quad (13)$$

where N is the number of sub-intervals, and $(\varepsilon_m +)_j^i$ and λ_j^i are the values of strain and probability density at the j -th quadrature point of the i -th sub-interval. w_j^i is the weight coefficient at the j -th quadrature point over the i -th sub-interval, which is determined by Gaussian quadrature.

Besides, it is presumed in the current model that the variation of the parameter T_M is characterized by the normal distribution. The normal density function λ needs to be calibrated from experimental measurement. Two aforementioned statistical coefficients μ and η in equation (8) are estimated from the phase transformation temperatures as

$$\mu = \frac{M_s^0 + M_f^0}{2}, \quad (14-a)$$

$$\eta = \frac{M_s^0 - M_f^0}{4}, \quad (14-b)$$

where M_s^0 and M_f^0 are the martensitic start temperature and the martensitic finish temperature in the stress-free experiment.

One of the superiorities of the proposed model is the low computational cost in numerical implementation. Firstly, the computation cost is reduced with the single-crystal model, where equation (5) is expressed as an ODE. As mentioned above, the governing ODE is solved by the trapezoidal method. Compared with the PDE models, it is always computationally easier to find the numerical solution for an ODE. Secondly, instead of using other homogenization techniques, the polycrystalline response is discretized as the weighted superposition in equation (13). The weights and other coefficients are pre-specified rather than estimated by optimization. Thirdly, only six model parameters need to be identified to construct the polycrystalline hysteresis loop, which also saves the computational cost.

4.2. Prediction of incomplete transitions

As mentioned in Section 1, most of the existed prediction strategies for incomplete transitions rely on the estimation of the phase volume fraction, which is associated with the evolution of internal variables. The prediction for partial transitions often requires computational efforts. Motivated by the scaling policy (Rizzello et al., 2019), the concept of density reassignment is introduced in this section to improve computational efficiency. Compared with the scaling policy, it

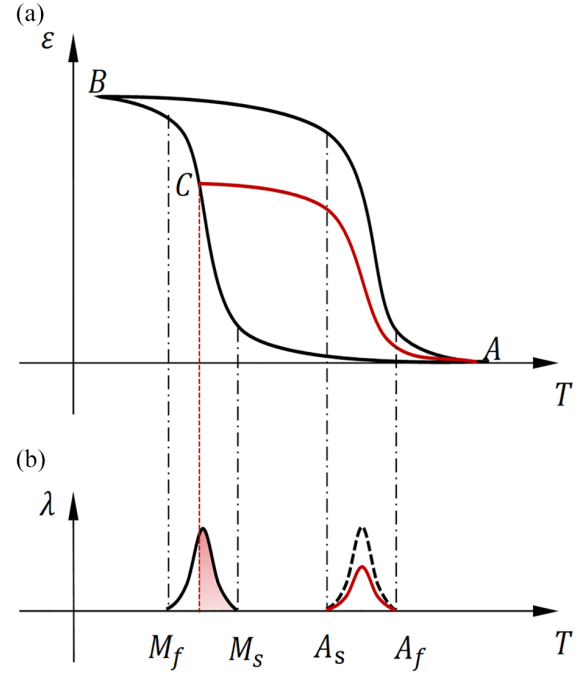


Figure 6. (a) An illustration of incomplete $A \rightarrow M$ transition and (b) the concept of “density reassignment”.

should be highlighted that the proposed strategy of density reassignment not only comes from the geometrical consideration of the internal loops but also enriches the physical aspects of the prediction.

When a polycrystalline SMA specimen is subjected to partial thermal cycles, it undergoes incomplete phase transition. In this section, a direct prediction strategy for incomplete transitions is presented and the incomplete $A \rightarrow M$ transformation is deployed for illustration. As is shown in Figure 6(a), the configuration of the polycrystal is 100% austenite at point A. The volume fraction of martensite increases at the expense of austenite with the drop of the material temperature and reaches 100% at point B. Then the austenitic transformation initiates as the material temperature rises and the 100% austenite configuration will be restored at point A.

As is presumed above, the temperature at which phase transformation occurs varies among the polycrystalline SMA, and the distribution property of the transformation temperatures is illustrated in Figure 6(b). If the thermal loading is reversed at an intermediate configuration (point C), the martensitic transformation terminates and the austenitic transformation initiates. During the cooling branch AC, the whole martensitic transformation has not finished yet. The volume fraction of the martensite is taken as ξ_M at the reversed point C. The ratio $\xi_M \in [0, 1]$ is introduced to quantify the phase transition process, which plays an important part in the prediction for incomplete transitions. For the incomplete $A \rightarrow M$ transformation, the remnant

austenite is assumed to be undisturbed by cooling and afterward heating. That is, the strain results from the austenitic transformation of the martensite as the material is heated again. Since the configuration at the reversed point C differs from that of point A , the developed stress field differs as well, leaving the austenitic transformation temperatures redistributed over the heating branch, as is shown in Figure 6(b). It is assumed that the reassigned density function takes the simplest form

$$\tilde{\lambda}(x) = f(\xi_M)\lambda(x), \quad (15)$$

where $f(\xi_M)$ is the configuration-dependent scaling factor. Some requirement on the scaling factor $f(\xi_M)$ need to be claimed as follows:

- (1) $f(\xi_M)$ is an increasing function defined for $0 < \xi_M < 1$,
- (2) $0 < f(\xi_M) < 1$.

For simplicity, it is specified as the following form,

$$f(\xi_M) = 1 - \alpha e^{-\gamma \xi_M}, \quad \alpha > 0, \quad \gamma > 0. \quad (16)$$

where α and γ are the constants that constitute the description of the scaling factor. Thus, the first-order reversal curves can be obtained via the utilization of the reassigned density function. Similar manipulation can be carried out to predict the first-order reversal curves for cases of the incomplete $M \rightarrow A$ transformation by estimating the austenitic volume fraction ξ_A at the reversed point and substituting it into equation (15) as $\xi_M = 1 - \xi_A$. It should be noted that the scaling factor $f(\xi_M)$ only depends on the current material configuration at the latest reversed point and is insensitive to the loading history, which makes the idea of density reassignment possible to be extended for higher-order reversal curves.

As mentioned above, the reversal curves after the incomplete transitions are predicted by density reassignment, which is the novelty of the proposed prediction strategy. The concept of density reassignment relies on the assumption of normally distributed transformation temperatures in the SMA polycrystals. For incomplete transitions, the density function of the transformation temperatures is modified by the scaling factor that is based on the phase volume fractions at the latest reversed point. Instead of coping with the evolution of the internal variables, the reversal curves are obtained with the scaled density function, which is equivalent to estimating the reversal curves by scaling the major loop. The main advantage of the proposed method is that the prediction of incomplete transitions is easily implemented with accuracy and efficiency. Even if the scaling factor reflects the physical assumption on the thermally-induced phase transitions, it

Table 1. The model parameters calibrated from the experimental data.

Description	Values	
	Maletta et al. (2008)	Nascimento et al. (2009)
a_2	2.32×10^5	6.11×10^4
a_4	1.97×10^{10}	6.59×10^9
a_6	1.06×10^{13}	2.49×10^{12}
τ	0.0724	0.166
β_0	0.808	—
k_σ	8.86×10^{-4}	—
μ	57.5	18.1
η	4.25	4.48

should be pointed out that the scaling idea comes from the observation of the self-similar pattern in reversal curves. Equation (16) simply provides a guess for the scaling factor. The mathematical expression of the scaling factor could be modified to improve the prediction accuracy.

5. Results and discussion

In this section, the experimental data in Maletta et al. (2008) and Nascimento et al. (2009) are employed to validate the model capability in the simulation of the strain-temperature hysteresis and the prediction of incomplete transitions. The experimental data in Maletta et al. (2008) are adopted to demonstrate the stress-dependent property of the proposed model and check the validity in the prediction of incomplete transitions. A trained bone-shaped Ni-Ti specimen is subjected to thermal cycles to study the thermally-induced hysteresis under different bias stresses. In this paper, the experimental data of the stress-free case and the stress-assisted case of 100 MPa are used to calibrate the model parameters and the calibrated model parameters are provided in Table 1. The case under the bias stress of 50 MPa is simulated with the same model parameters to examine the stress dependence of the proposed model. As shown in Figure 7, the model predictions are compared with the experimental measurement as well as the model results in Maletta et al. (2008). It can be seen that both the transformation temperatures and the maximum deformation increase as the bias stress is elevated. The model prediction results agree well with the experimental counterparts in both the stress-free case and stress-assisted cases, exhibiting similar trends. The root-mean-square error between the measured strain value and the predicted counterpart is employed to evaluate the modeling accuracy. The root-mean-square strain errors of the model prediction under three bias stresses are 1.653×10^{-3} , 1.868×10^{-3} , and 3.597×10^{-3} , respectively. Good agreement indicates that the presented model and the selection of

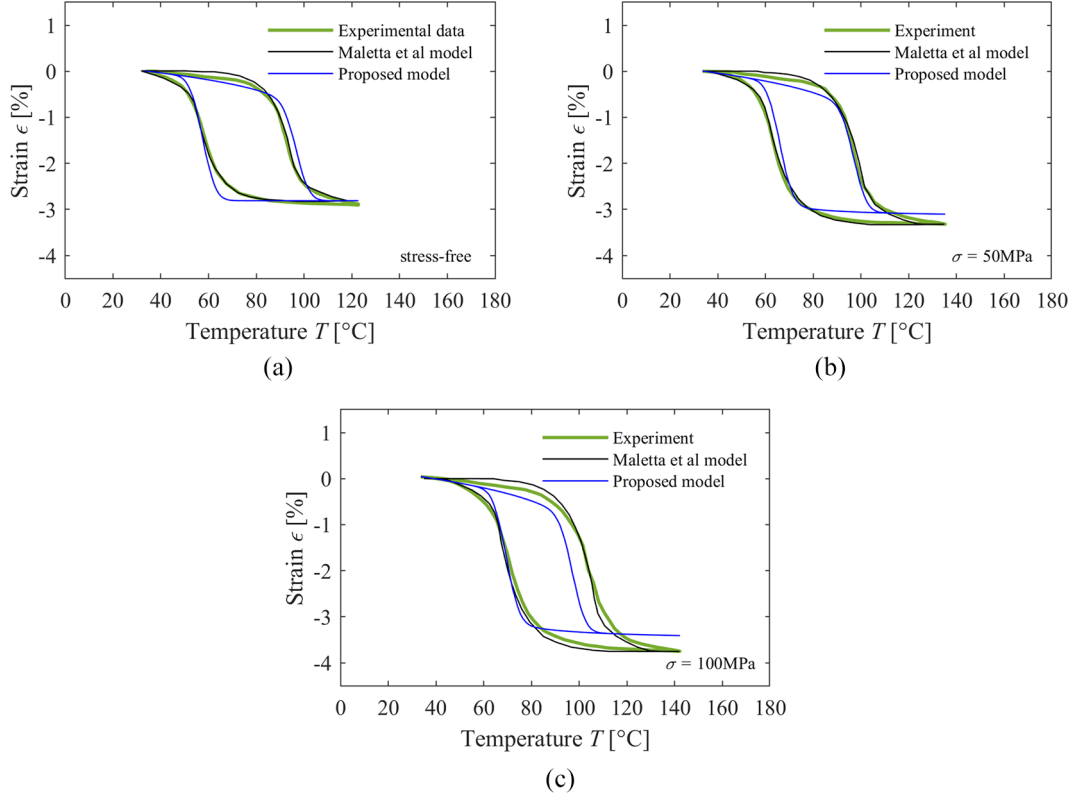


Figure 7. Comparisons between the model predictions and the experimental data as well as the model results in Maletta et al. (2008) under: (a) 0 MPa, (b) 50 MPa, and (c) 100 MPa.

normal density function exhibits accuracy and adaptability in capturing polycrystalline hysteresis. However, discrepancies still exist in comparison with experimental results when bias stress is elevated to 100 MPa. It is worth noting that the modified Prandtl-Ishlinskii model (Maletta et al., 2008) and the proposed model share a similar strategy, which is to construct the major hysteresis loop as the weighted superposition of elementary units. The main differences between these two studies lie in the form of the elementary unit and the identification of the weights. Firstly, the elementary unit in the proposed model is derived from the differential single-crystal unit. The differential form of the elementary unit is the novelty of the current model, which enriches the physical significance of the modeling and benefits the control of the strain-temperature hysteresis. Secondly, the weights in the current model are determined based on the assumption of normally-distributed transformation temperatures, leaving only six model parameters to be identified. The proposed model addresses the hysteresis on the basis of the energy description. Compared with the former modeling strategy, the computational efficiency and the inherent stress-dependent property are the superiorities of the current model.

The predicted first-order reversal curves are plotted in Figure 8, in comparison with the experimental data

and the model results in Maletta et al. (2008). Coefficients $\alpha = 0.820$ and $\gamma = 1.75$ are determined from the experiment of incomplete $A \rightarrow M$ transformation in Figure 8(a), and are used to predict the minor loops for incomplete $M \rightarrow A$ transformation in Figure 8(b) afterward. The root-mean-square strain error for the incomplete $A \rightarrow M$ transformation is 1.347×10^{-3} while the counterpart for the incomplete $M \rightarrow A$ transformation is 5.064×10^{-3} . It can be seen in Figure 8 that the proposed prediction scheme generally well captures the first-order reversal curves in both cases via the strategy of density reassignment. Besides, the experimental data in Nascimento et al. (2009) are also presented to examine the model capability in the prediction of the first-order reversal curves, where the strain-temperature hysteresis loops of an equiatomic Ni-Ti wire actuator are studied. The comparison between the model predictions and the experimental results as well as the model results in Nascimento et al. (2009) is shown in Figure 9. Although the stress-free transformation temperatures are not provided in the reference, they can be estimated from the hysteresis responses under several applied loads. For convenience, $\beta = 1$ and the identified parameter set used for the prediction of major hysteresis loop under 200 MPa is listed in Table 1. The coefficients $\alpha = 0.890$ and $\gamma = 1.18$ are calibrated from these incomplete

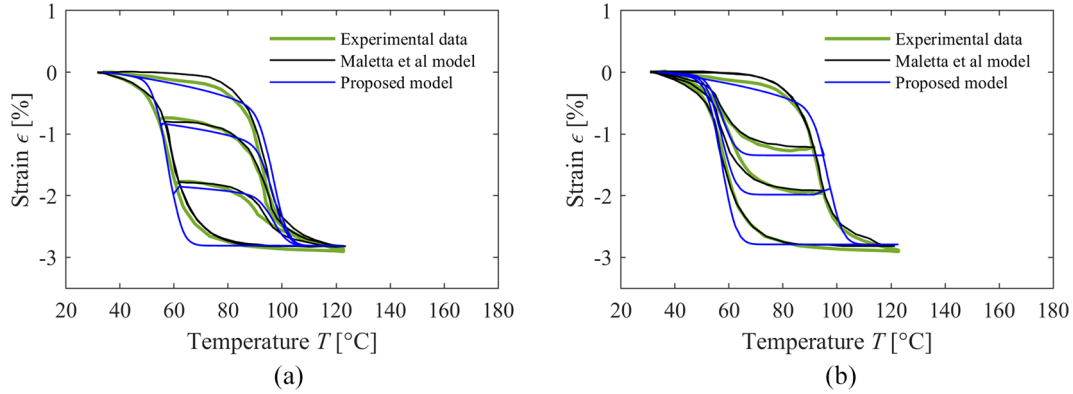


Figure 8. Comparisons between the model predictions and the experimental data as well as the model results in Maletta et al. (2008) for stress-free incomplete transitions: (a) incomplete $A \rightarrow M$ transition and (b) incomplete $M \rightarrow A$ transition.

transitions. It can be seen that the prediction results exhibit qualitative agreement with the experimental data. The root-mean-square strain errors for the major loop and first-order reversal curves are 2.658×10^{-3} and 1.093×10^{-3} . Herein, the choice of scaling factor $f(\xi_M)$ is simply out of convenience and the prediction results could be improved by other choices. Compared with other studies, the proposed prediction method for internal loops comes from both the geometrical observation and the physical assumption. As mentioned in Section 4.2, the strategy of density reassignment is the novelty of the current study in prediction of incomplete transitions.

It can be seen in Figures 7 to 9 that the stress-dependent property and the internal-loop pattern are well captured by the proposed model. Compared with previous models, the computational efficiency of the proposed model is improved, but the modeling accuracy is compromised. Large discrepancies still exist between the experimental data and the model predictions. In the current model, the discrepancies mainly arise from two aspects. Firstly, the discrepancies result from the strong nonlinearity in the Landau free energy function that is given by a 2-4-6 polynomial as equation (1). The high-order polynomial ensures the nonlinearity in the proposed model. However, excessive nonlinearity may cause discrepancies in the model prediction. Thus, one way to improve the accuracy is to modify the Landau free energy function into a lower-order form. Secondly, the discrepancies arise from the presumed density function. In the proposed model, the normal density function is employed for convenience. The discrepancies could be reduced with other probability density functions or density estimation determined by direct curve-fitting. Besides, it is worth noting that the prediction accuracy of incomplete transitions depends on the accuracy of the predicted outer hysteresis loop. The modeling accuracy of the internal loops will be enhanced if the discrepancies in the outer loop are reduced.

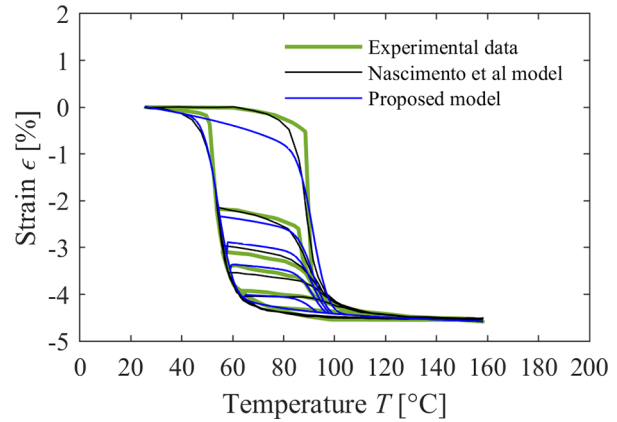


Figure 9. Comparisons between the model predictions and the experimental data as well as the model results in Nascimento et al. (2009) for incomplete $A \rightarrow M$ transitions under 200 MPa.

6. Conclusions

In this work, a differential single-crystal hysteresis unit is developed via the TDGL equation and formulated in an ODE. Based on the assumption of the distributed transformation temperatures, the polycrystalline response is constructed as the weighted combination of single-crystal hysteresis units, and the distribution property is characterized by the normal density function. Numerical procedure is stated clearly and implemented to determine the model parameters from the experimental data. The idea of density reassignment is discussed and deployed to predict the minor hysteresis pattern of incomplete transformation. The experimental results of SMA polycrystals are utilized to demonstrate the polycrystalline model's capability of capturing thermally-induced hysteresis and verify the proposed prediction strategy for incomplete transitions. Both the model simulations and predictions exhibit good accuracy, revealing the effectiveness of the presented phenomenological model and the prediction strategy. Besides, the presented model is formulated in the ODE form and

easily implemented, which can benefit the engineering applications and control issues of thermally-induced phase transitions in SMA polycrystals.


Declaration of conflicting interests

The authors declared no potential conflicts of interest with respect to the research, authorship, and/or publication of this article.

Funding

The authors disclosed receipt of the following financial support for the research, authorship, and/or publication of this article: This work has been supported by the National Natural Science Foundation of China (Grant No. 51575478 and Grant No. 61571007). R. Melnik acknowledges the support from the NSERC and CRC program.

ORCID iD

Yuxiang Han  <https://orcid.org/0000-0003-1312-0258>

References

- Bartel T, Osman M and Menzel A (2017) A phenomenological model for the simulation of functional fatigue in shape memory alloy wires. *Meccanica* 52(4–5): 973–988.
- Bhattacharyya A and Lagoudas DC (1997) A stochastic thermodynamic model for the gradual thermal transformation of SMA polycrystals. *Smart Materials and Structures* 6(3): 235–250.
- Bo Z and Lagoudas DC (1999) Thermomechanical modeling of polycrystalline SMAs under cyclic loading, part IV: Modeling of minor hysteresis loops. *International Journal of Engineering Science* 37(9): 1205–1249.
- Chemisky Y, Duval A, Patoor E, et al. (2011) Constitutive model for shape memory alloys including phase transformation, martensitic reorientation and twins accommodation. *Mechanics of Materials* 43(7): 361–376.
- Chemisky Y, Hartl DJ and Meraghni F (2018) Three-dimensional constitutive model for structural and functional fatigue of shape memory alloy actuators. *International Journal of Fatigue* 112: 263–278.
- Cissé C and AsleZaeem M (2020a) An asymmetric elastoplastic phase-field model for shape memory effect, pseudoelasticity and thermomechanical training in Polycrystalline shape memory alloys. *Acta Materialia* 201: 580–595.
- Cissé C and AsleZaeem M (2020b) On the elastocaloric effect in CuAlBe shape memory alloys: A quantitative phase-field modeling approach. *Computational Materials Science* 183: 109808.
- Crews JH, Smith RC, Pender KM, et al. (2012) Data-driven techniques to estimate parameters in the homogenized energy model for shape memory alloys. *Journal of Intelligent Material Systems and Structures* 23(17): 1897–1920.
- Daghia F, Fabrizio M and Grandi D (2010) A non isothermal Ginzburg-Landau model for phase transitions in shape memory alloys. *Meccanica* 45(6): 797–807.
- Dhote RP, Gomez H, Melnik RN, et al. (2015) 3D coupled thermo-mechanical phase-field modeling of shape memory alloy dynamics via isogeometric analysis. *Computers & Structures* 154: 48–58.
- Doraiswamy S, Rao A and Srinivasa AR (2011) Combining thermodynamic principles with Preisach models for superelastic shape memory alloy wires. *Smart Materials and Structures* 20(8): 085032.
- Dornelas VM, Oliveira SA and Savi MA (2020) A macroscopic description of shape memory alloy functional fatigue. *International Journal of Mechanical Sciences* 170: 105345.
- Falk F (1980) Model free energy, mechanics, and thermodynamics of shape memory alloys. *Acta Metallurgica* 28(12): 1773–1780.
- Falk F (1983) Ginzburg-Landau theory of static domain walls in shape-memory alloys. *Zeitschrift für Physik B Condensed Matter* 51(2): 177–185.
- Hao L, Qiu J, Ji H, et al. (2017) Numerical analysis on thermo-mechanical behavior of shape memory alloy strip with two-way shape memory effect. *Journal of Intelligent Material Systems and Structures* 28(16): 2298–2304.
- Heller L, Šittner P, Sedláč P, et al. (2019) Beyond the strain recoverability of martensitic transformation in NiTi. *International Journal of Plasticity* 116: 232–264.
- Li X and Su Y (2020) A phase-field study of the martensitic detwinning in NiTi shape memory alloys under tension or compression. *Acta Mechanica* 231(4): 1539–1557.
- Maletta C, Falvo A and Furguele F (2008) A phenomenological approach for real-time simulation of the two-way shape memory effect in NiTi alloys. *Journal of Engineering Materials and Technology* 130(1): 011003.
- Mamivand M, Zaeem MA and El Kadiri H (2013) A review on phase field modeling of martensitic phase transformation. *Computational Materials Science* 77: 304–311.
- Massad JE and Smith RC (2005) A homogenized free energy model for hysteresis in thin-film shape memory alloys. *Thin Solid Films* 489(1–2): 266–290.
- Nascimento MM, de Araújo CJ, de Almeida LA, et al. (2009) A mathematical model for the strain–temperature hysteresis of shape memory alloy actuators. *Materials & Design* 30(3): 551–556.
- Oliveira SDA, Dornelas VM, Savi MA, et al. (2018) A phenomenological description of shape memory alloy transformation induced plasticity. *Meccanica* 53(10): 2503–2523.
- Petrini L and Bertini A (2020) A three-dimensional phenomenological model describing cyclic behavior of shape memory alloys. *International Journal of Plasticity* 125: 348–373.
- Rao A, Ruimi A and Srinivasa AR (2014) Internal loops in superelastic shape memory alloy wires under torsion – Experiments and simulations/predictions. *International Journal of Solids and Structures* 51(25–26): 4554–4571.
- Rizzello G, Mandolino MA, Schmidt M, et al. (2019) An accurate dynamic model for polycrystalline shape memory alloy wire actuators and sensors. *Smart Materials and Structures* 28(2): 025020.
- Saleeb AF and Owusu-Danquah JS (2017) The role of residual stress states in modeling the cyclic two-way shape memory behavior of high-temperature NiTiPd alloys and actuation components. *Mechanics of Materials* 110: 29–43.
- Scalet G, Niccoli F, Garion C, et al. (2019) A three-dimensional phenomenological model for shape memory

- alloys including two-way shape memory effect and plasticity. *Mechanics of Materials* 136: 103085.
- She H, Liu Y, Wang B, et al. (2013) Finite element simulation of phase field model for nanoscale martensitic transformation. *Computational Mechanics* 52(4): 949–958.
- Xiao Y and Jiang D (2020) Constitutive modelling of transformation pattern in superelastic NiTi shape memory alloy under cyclic loading. *International Journal of Mechanical Sciences* 182: 105743.
- Xie X, Kang G, Kan Q, et al. (2019) Phase field modeling to transformation induced plasticity in super-elastic NiTi shape memory alloy single crystal. *Modelling and Simulation in Materials Science and Engineering* 27(4): 045001.
- Zhong Y and Zhu T (2014) Phase-field modeling of martensitic microstructure in NiTi shape memory alloys. *Acta Materialia* 75: 337–347.